Driving mechanisms for the formation of nanocrystals by annealing of ultrathin Ge layers in SiO_2

R. Peibst,[1,*] T. Dürkop,[1] E. Bugiel,[1] A. Fissel,[2] I. Costina,[3] and K. R. Hofmann[1,2]
[1]*Institute of Electronic Materials and Devices, Leibniz Universität Hannover 30167, Germany*
[2]*Information Technology Laboratory, Leibniz Universität Hannover 30167, Germany*
[3]*IHP Microelectronics, Frankfurt/O. 15236, Germany*
(Received 20 March 2008; revised manuscript received 25 March 2009; published 18 May 2009)

We investigated the transformation of ultrathin continuous amorphous Ge layers embedded in SiO_2 into isolated nanocrystals during thermal annealing. The dependence of the cluster self-organization processes on annealing time, annealing temperature, and initial layer thickness was studied quantitatively by extensive transmission electron microscopy analysis. The nanocrystal formation was found to run through distinct subsequent stages, from homogeneous crystal nucleation in the Ge layer to the outgrowth and ripening of isolated nanocrystals, within a few seconds for temperatures in the range of 1000 °C. The driving mechanisms of cluster formation were analyzed with a simple thermodynamic model of the Gibbs free energy. This indicates that the observed outgrowth of clusters from the initial layer into the SiO_2 is essentially driven by the relaxation of the nanocluster interface energy due to structural adaption of the Ge, yielding an energetic benefit of the transformation of the continuous initial layer into isolated clusters as compared to a simple layer recrystallization. The observed bimodal nanocrystal size distributions are tentatively explained by an additional contribution to the free energy yielding a second barrier in cluster evolution, which can be deduced from the experiments. It is possibly related to inelastic strain effects in the nanocrystal formation. Ripening effects of the nanocrystals turned out to be not limited by diffusion.

DOI: 10.1103/PhysRevB.79.195316 PACS number(s): 68.65.Hb

I. INTRODUCTION

During the last decade, semiconductor and metal nanocrystals (NCs) embedded in an insulating matrix have attracted a large number of researches due to their potential applications in optoelectronic and memory devices.[1–5] The most common material systems investigated have been Si or Ge NCs in a SiO_2 matrix, while other insulator or NC materials have been investigated as well.[6–8] The NC size of a few nanometers requires a self-organization process for preparation. For an optimization of the structural parameters of the NCs as well as for an integration of the self-organization step into a standard process for device fabrication, an understanding of the driving forces of the NC formation is essential.

For Ge NCs embedded in SiO_2, one may roughly classify most of the different preparation methods according to the type of self-organization: either segregation of Ge from Ge enriched SiO_2 (Ge/Si alloys) or transformation of a continuous embedded Ge layer into isolated NCs. In the first case, NC formation occurs during an annealing step after ion implantation of Ge into the SiO_2,[9,10] cosputtering of Ge and SiO_2,[11,12] depositing Si_xGe_{1-x} alloys by plasma-enhanced chemical vapor deposition (PECVD),[13] or during oxidation of Si_xGe_{1-x} alloys.[14,15] For these systems, there are a few reports addressing the role of chemical reactions,[3,12] of Ge diffusion in the SiO_2 matrix,[11] and of the influence of the annealing time and temperature[13] on the NC formation. The second type of self-organization, i.e., the transformation of a continuous embedded Ge layer into isolated clusters by thermal annealing, is not well understood so far. This type of self-organization does not seem to occur for α-Si layers embedded in SiO_2. For $SiO_2/\alpha\text{-Si}/SiO_2$ superlattices, Zacharias and Streitenberger[16] reported an increase in the recrystallization temperature with decreasing α-Si layer thickness, but NC formation was restricted to the initial layer. After annealing of $SiO_2/\alpha\text{-Si}/SiO_2$ superlattices, Grom *et al.*[17] observed rather brick-shaped or elliptical Si NCs still contained in continuous layers and restricted to the initial layer thickness in the vertical dimension.

The formation of NCs with diameters larger than the initial layer thickness and a subsequent dissolution of the initial layer was described qualitatively by Heng *et al.*[18,19] for the $SiO_2/\alpha\text{-Ge}/SiO_2$ system. Their samples apparently contained a large amount of GeO_x, which was reduced to elementary Ge during NC formation.

In this work, we aim at an analysis of the driving forces of the NC formation from a thin continuous layer of elementary Ge embedded in SiO_2. The dependence of the self-organization on annealing time, temperature, and layer thickness is studied quantitatively by extensive transmission electron microscopy (TEM) analyses including the evolution of the distribution of the intercluster distances and of the NC size distributions. We will show that the NC formation process can be classified into distinct subsequent stages of which each is dominated by one particular mechanism. A thermodynamic model will be presented which provides a simple explanation for the observed effects, including the outgrowth of the NCs from the initial Ge layer.

II. EXPERIMENTAL

The samples investigated for nanocrystal formation consisted of an ultrathin layer of elementary Ge sandwiched between top and bottom SiO_2 layers on a Si substrate. For their preparation, we have developed recently[20] a PECVD deposition process of amorphous Ge on the bottom SiO_2, using an

TABLE I. Investigated samples, annealing conditions, and resulting NC parameters. The maximum error is 0.3 nm for the mean nanocrystal diameter, 0.2 nm for the layer thickness d_0, $0.2 \cdot 10^{11}$ cm^{-2} for the nanocrystal areal density, 0.5 nm for the cluster distances L_{typ} and S_{typ}, and 0.4 nm for the peak positions of $\nu(r_{nc})$. The maximum error for the peak ratio a_1/a_2 is 25% of the absolute value. (⋆ increase in the recrystallization temperature supposed, † no isolated NCs resolvable, ⋆⋆ no nanocrystal formation, and ‡ no bimodal frequency distribution observed).

Sample	1	2	3	4	5	6	7	8	9	10	11	12
Ge layer thickness d_0 [nm]	2.3	2.3	2.4	2.5	2.5	2.5	2.5	2.5	2.5	2.7	2.7	8.4
Annealing parameters (s), °C	20, 1020	20, 1030	30, 950	180, 750	20, 850	20, 900	20, 950	10, 950	7, 1000	5, 1020	20, 1020	600, 750
Attributed stage of NC formation	2⋆	2⋆	2–3	1–2	2	2	2–3	2	2	2	3	⋆⋆
Cluster density $n[10^{11}cm^{-2}]$	4.8	4.9	4.4	†	4.8	4.2	4.2	6.9	6.0	4.7	2.2	⋆⋆
Mean cluster radius $\langle r_{nc} \rangle$ [nm]	2.3	2.6	2.9	†	2.9	3.6	3.5	2.7	2.9	3.1	5.3	⋆⋆
Intercluster distance L_{typ} [nm]	7.4	7.4	8.2	†	7.2	7.4	7.3	6.7	6.4	6.8	11.5	⋆⋆
Distance S_{typ} between the NC centers [nm]	12.7	12.8	15.6	†	13	14.3	13.9	13.4	13.1	13.4	24.5	⋆⋆
Peak ratio a_1/a_2 of $\nu(r_{nc})$	0.339	0.06	0.064	†	0.124	0.098	0.02	0.55	‡	‡	‡	⋆⋆
Position of the first/second peak of $\nu(r_{nc})$ [nm]	1.7/2.6	1.5/2.7	1.4/3	†	1.2/3	1.7/3.6	1.5/3.4	1.6/3.4	‡	‡	‡	⋆⋆

Oxford Plasmalab 90 PECVD system. The Ge layers were capped by PECVD *in situ* with the top SiO_2, avoiding any exposure of the Ge to environmental influences, in particular, to oxygen and to air humidity. We used *p*-type (100) Si as substrate, dry thermal oxidation at 850 °C for the growth of the bottom oxide layer with a thickness of 4 nm, GeH_4 as precursor for the Ge deposition at 200 °C, and SiH_4 and N_2O as precursors for the deposition of a 12 nm top SiO_2 layer at 400 °C. More details of the sample preparation can be found in the work of Dürkop *et al.*[20]

The thicknesses d_0 of the as-prepared Ge layers were determined by spectroscopic ellipsometry using a *SENTEC SE 800*. These measurements were calibrated and confirmed by numerous cross-section TEM images of the as-prepared layer stack.

In the present investigation we studied the influence of the initial layer thickness d_0 on NC formation in the thickness range of 2.3–8.4 nm. To eventually transform the continuous initial layer into isolated NCs, the samples were annealed at different temperatures between 750 and 1020 °C, with a variation in annealing time from 5 to 600 s (see Table I).

The annealing was performed in a rapid thermal processing machine (*AST SHS 100*) in Ar atmosphere with fixed heating/cooling ramps of 60 °C s^{-1}. After reaching its maximum value, the annealing temperature was kept constant for the annealing times listed in Table I. The temperature was controlled by a pyrometer located underneath the sample and calibrated by Pt/Pt-Rd thermocouples embedded in a calibration wafer. On this calibration wafer, a layer stack of $SiO_2/Ge/SiO_2$ equal to that of our samples was deposited in order to obtain the same absorption and emission properties. By comparing the thickness of SiO_2 layers grown by dry thermal oxidation on pure Si substrates with respective models,[21] we determined that the error in the temperature control was smaller than ± 5 K and found an excellent wafer to wafer reproducibility.

The as-prepared layer composition was analyzed by x-ray photoelectron spectroscopy (XPS) profiling [Fig. 1(a)]. Profiles were acquired with a *Physical Electronics PHI 5600* system by monitoring the O 2*p*, Si 2*p*, and Ge 3*p* photoemission after 60 s sputtering cycles (Ar^+ ions at 2 keV). Single element sensitivity factors from the spectrometer database (*Multipak 8.2*) were used to estimate the concentrations.[22] Since the depth resolution of the XPS measurements is limited (≈2–3 nm), the Ge layer thickness d_0 was increased to 15 nm for these investigations. Such Ge layers recrystallize during annealing as continuous layers rather than forming isolated NCs. As shown in Fig. 1(a), we observed a concentration of nearly 100% of elementary Ge within the as-prepared layer. This could be attributed to the *in situ* capping of the Ge layer, as well as to the temperature for the top SiO_2 deposition (400 °C). This temperature is high enough to evaporate any GeO_x formed initially on the Ge layer. Because the GeO_x content is negligibly small in our samples and Ge is known to be stable in SiO_2,[23] we conclude that chemical reactions are of minor influence for the nanocrystal formation. An XPS profile of an annealed sample is shown in Fig. 1(b). Within the detection accuracy, no interdiffusion of Ge and SiO_2 or Si from the substrate was observed. The stack structure was maintained. This is surprising since the annealing temperature was 80 K higher than the melting point of bulk Ge (937 °C). However, it is consistent

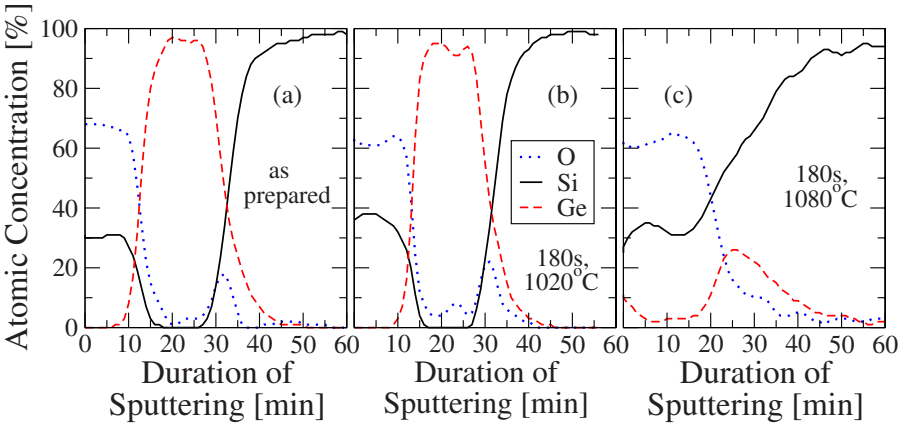

FIG. 1. (Color online) (a) XPS profile of an as-prepared sample with a 15-nm-thick Ge layer on native silicon dioxide, capped with 12 nm SiO_2. (b) XPS profile of the same sample annealed at 1020 °C for 180 s. (c) Equivalent sample after annealing at 1080 °C for 180 s.

with the observation of a large melting point temperature increase of about 160 K recently reported for Ge nanostructures embedded in SiO_2.[24] Our results seem to substain this observation. For the larger annealing temperature of 1080 °C, the stack structure was dissolved [Fig. 1(c)]. We suppose that the Ge layer was molten in this case. All samples investigated in this work were annealed at $T \leq 1020$ °C, i.e., below the observed melting point of the Ge nanostructures embedded in SiO_2.[24] Therefore, we assume that no melting of the embedded Ge occurred in our experiments.

The TEM investigations were carried out on a *JEOL JEM 2100F* at 200 keV. The sample preparation includes mechanical dimpling as a first step and ion thinning as a second step.[25] The techniques for planview observation were bright field, high resolution, and selected area diffraction. For each sample, four planview TEM images at different locations were analyzed, corresponding to about 500 NCs, in order to obtain statistically significant results. The first step of the computerized analysis was a conversion of the TEM planview images into binary (black and white) images by filtering and defining a certain threshold gray level. Then, a cluster detection algorithm was applied to determine the projected area and the lateral positions of the NCs. For each image, the accuracy of the cluster detection was checked visually. The NC radii were obtained by approximating the NC shape by a sphere ($r_{nc} \approx \sqrt{A_{projected}/\pi}$). The areal density of the NCs was obtained by dividing the total number of NCs by the total area imaged.

We also performed scanning electron microscopy (SEM) investigations of samples where the top oxide was removed by wet chemical etching using a *Zeiss DSM 982 Gemini*. Although the average size of the NCs is slightly below the reliable resolution of our instrument (≈30 nm for these types of samples), SEM offers the possibility of observing the lateral distribution of the Ge remaining between the NCs due to a specific contrast for different elements (Sec. III C). For the top oxide removal, a 0.25% Hydrogen fluoride (HF) solution was used with etching rates of 3.5 nm/min for SiO_2 and ≪0.1 nm/min for Ge. A low electron energy of 2 keV was used to minimize charging effects.

III. RESULTS AND DISCUSSION

A. General processes of nanocrystal formation

In our experiments, we could not detect any formation of amorphous Ge clusters in spite of extensive TEM investigations covering the range of samples and annealing parameters given in Table I. We found only crystalline clusters (NCs). This finding forms the basis of our further analyses below. In high-resolution transmission electron microscopy (HRTEM) images, one can observe lattice fringes for all clusters investigated [Figs. 2(b)–2(d)]. The observed electron diffraction pattern (not shown) provided further evidence for crystalline nanoclusters. In planview TEM images, examples can be seen in Figs. 2(c) and 2(d); the clusters exhibit different gray levels originating from their different orientations to the incident electron beam. When changing the angle of incidence, the contrast of each cluster was found to change. This fact clearly indicates that the clusters are crystalline. Therefore, we concluded that crystal nucleation triggers the cluster formation rather than the endeavor to minimize the Ge/SiO_2 interface, which would yield amorphous Ge clusters as well. This basic assumption can be supported by a general argument. Assuming Ge/SiO_2 interface minimization to be the exclusive driving mechanism for NC formation, one can formulate a balance of the Ge/SiO_2 interface for the case of a simple recrystallization of the continuous α-Ge layer and for the case of a transformation of the initial layer into isolated clusters. In this picture, the kinetic pathway of NC formation is energetically advantageous as long as the following condition holds:

$$2A > N4\pi\langle r_{nc}\rangle^2. \tag{1}$$

Here, A denotes an arbitrary area of the initial layer with a thickness of d_0, which is transformed into N nanoclusters with a mean radius $\langle r_{nc}\rangle$. Eliminating $n=N/A$ by using volume conservation,

$$d_0 A = N\frac{4}{3}\pi\langle r_{nc}\rangle^3, \tag{2}$$

yields

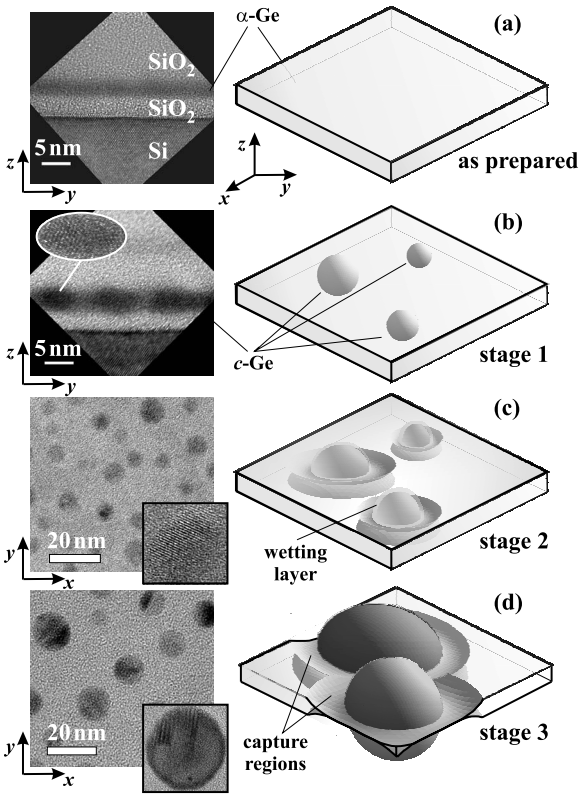

FIG. 2. Different stages of NC formation (a) cross-section TEM image of an as-prepared sample and illustration of the initial amorphous Ge layer (b) cross-section TEM image of sample 4 and illustration of stage 1 (nucleation within the Ge layer), (c) planview TEM image of sample 10 and illustration of stage 2 (outgrowth of the NCs from the initial layer), and (d) planview TEM image of sample 11 and illustration of stage 3 (ripening). The insets in (b)–(d) show an enlarged view of NCs imaged in high resolution.

$$\langle r_{\mathrm{nc}} \rangle > \frac{3}{2} d_0. \tag{3}$$

Most of our samples showing isolated nanocrystals do not fulfill condition (3). At the beginning of the outgrowth from the initial layer, the mean NC radius is $d_0/2$. For this case, no energetic benefit would be obtained by the outgrowth according to Eq. (3). Therefore, the transformation of the continuous layer into isolated nanocrystals cannot be explained exclusively by the minimization of the Ge/SiO_2 interface.

Based on this consideration, as well as on our extensive experimental observations, we classified the formation processes of the NCs into the following three stages which were subsequently observed with increasing annealing time:

(i) initial stage: the initial amorphous Ge layer is continuous and exhibits rather flat interfaces to the top and bottom oxide [Fig. 2(a)];

(ii) stage 1: within the initial Ge layer, crystal nuclei start to form by homogeneous nucleation [Fig. 2(b)]. This process is driven by a decrease in the total Gibbs free energy due to the transformation of amorphous Ge into crystalline Ge (Sec. III B).

(iii) Stage 2: the size of the NCs exceeds the initial layer thickness and they expand into the SiO_2. During the outgrowth, the crystalline Ge seems to be separated from the SiO_2 by a wetting layer of amorphous Ge whose formation is driven by a minimization of the Gibbs free energy of the Ge/SiO_2 interface (Sec. III B). This wetting layer of α-Ge provides the material required for the outgrowth of the NC from the initial layer. While Ge from the wetting layer is continuously incorporated into the NC during further growth, the material necessary to maintain the wetting layer is drawn from a circular capture region surrounding each crystal [Fig. 2(c)]. In the limit of large annealing times, the continuous initial layer is almost completely transformed into isolated clusters. The SiO_2 matrix adapts itself to the Ge structure.

(iv) Stage 3: when the capture regions of neighboring crystals start to overlap, a ripening of the nanocrystals occurs [Fig. 2(d)]. Larger NCs grow at the expense of smaller ones driven by the endeavor to minimize the total Ge/SiO_2 interface area and therefore the Gibbs free energy (Sec. III C), a process that is known as Ostwald ripening.[26]

These findings differ significantly from results reported for comparable SiO_2/α-Ge/SiO_2 and SiO_2/α-Si/SiO_2 systems.[16–19] During annealing of α-Si layers embedded in SiO_2, nanocrystals were formed, but no outgrowth from the initial layer was observed.[16,17] As we will argue below, the high specific c-Ge/SiO_2 interface energy and its relaxation by structural adaptation of the Ge seem to play an essential role for the outgrowth of the NCs from the initial layer. We believe that these effects are less effective in the SiO_2/α-Si/SiO_2 system. For α-Ge layers embedded in SiO_2, Heng *et al.*[18,19] reported a similar behavior as obtained for our samples, but also observed the formation of amorphous nanoclusters. However, there was a large amount of GeO_x in their samples, possibly due to ambient exposure after electron beam evaporation of Ge. It seems that GeO_x can also form agglomerations in SiO_2. Due to the *in situ* capping of our Ge layers, the amount for GeO_x is very small in our samples (compare Sec. II). Therefore no amorphous nanoclusters were formed, and reduction of GeO_x to elementary Ge by Si plays a minor role in our samples.

B. Nucleation and outgrowth of the nanocrystals (stages 1 and 2)

As mentioned above, crystal nucleation within the initial amorphous layer is the first stage of NC formation, which was observed for temperatures above 750 °C. In HRTEM images [e.g., Fig. 2(b)], we found the Ge crystal nuclei to be preferentially located in the middle of the Ge layer rather than at the Ge/SiO_2 interfaces. We therefore believe that the nucleation is homogeneous rather than heterogeneous. Homogeneous nucleation in bulk material can be described within the framework of classical nucleation theory (for a review, see Ref. 27). Within this approach, the nuclei density n depends almost linear on the annealing time. Considering a thermally activated nucleation rate j per unit volume, the nanocrystal areal density is expected to be given by

$$n = j_0 \exp\left(-\frac{\Delta G_1^*}{k_B T}\right) d_0 t. \tag{4}$$

Here, d_0 denotes the initial layer thickness, and ΔG_1^* is the activation energy for homogeneous nucleation. Figure 3

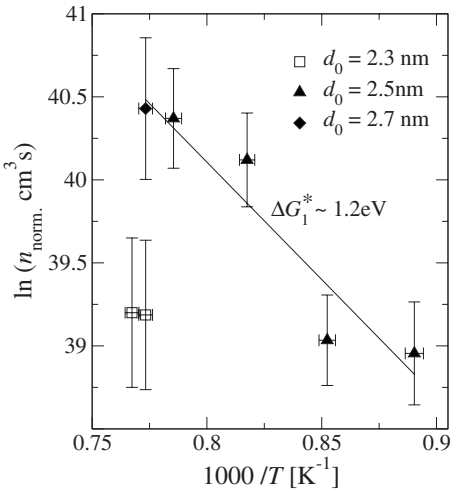

FIG. 3. Arrhenius plot of the NC area density n, normalized to the annealing time and the initial Ge layer thickness. The data plotted originate from samples 5, 6, 8, 9, and 10. These samples are assumed not to have transited from stage 2 to ripening stage 3.

shows an Arrhenius plot of the normalized areal NC density $n_{\mathrm{norm}}=n/(d_0 t)$ for all samples which are assumed not to have transited to the ripening regime yet (Table I). For each sample, this classification is essentially based on a comparison of the NC areal density with values obtained by different annealing times for otherwise the same parameters, as well as on the shape of the frequency distribution of the NC radii (see below).

For $d_0 \geq 2.5$ nm, i.e., for sample 5, 6, 8, 9, and 10, n_{norm} exhibits an Arrhenius behavior. The slope of the fitted line yields an activation energy $\Delta G_1^*=(1.2\pm0.1)$ eV, and a prefactor $j_0=(2.14\pm0.2)10^{22}$ cm^{-3} s^{-1}. However, for samples 1 and 2 with $d_0=2.3$ nm, n_{norm} is significantly smaller than the value expected by an extrapolation of the behavior of the samples with a larger initial layer thickness. This observation does not necessarily contradict Eq. (4). Rather, it can be interpreted in terms of an increase in the recrystallization temperature with decreasing d_0, a well-known effect found by Williams *et al.*[28] and Zacharias and Streitenberger[16] to occur in ultrathin Si and Ge films embedded in SiO_2.

In Refs. 16 and 28, however, only the nucleation within the initial layers and not the outgrowth of the crystal nuclei from the initial layers was investigated, which was the main objective of our TEM investigations. The experimental findings of this stage of NC formation are presented in the following.

A HRTEM cross-section image of sample 4, which is transiting from the growth mode within the initial layer to the outgrowth from it, is shown in Fig. 4(a). The average vertical size of the crystals roughly corresponds to the initial layer thickness of 2.5 nm. Obviously, the NCs are encased in an intermediate layer of amorphous Ge, separating the c-Ge from the SiO_2. This local agglomeration of Ge causes a roughening of the α-Ge/SiO_2 interface, which is flat in the as-prepared stage [Fig. 2(a)]. An intermediate layer of amorphous Ge between the nanocrystal and the SiO_2 matrix can also be observed for other samples exhibiting small NCs, but it vanishes for large NC radii. The structural parameters of

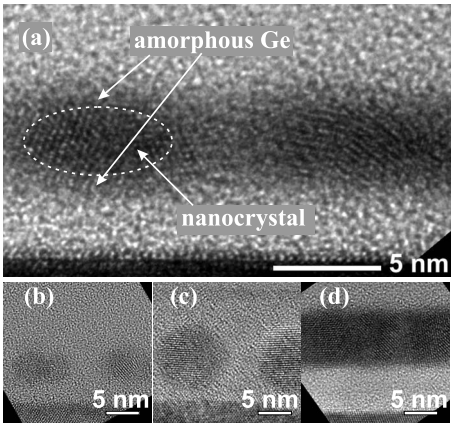

FIG. 4. (a) Cross-section TEM images for sample 4 showing the transition of the NC growth within the initial layer to the outgrowth from it. (b)–(d) Influence of the initial Ge layer thickness d_0 on the NC formation behavior. Cross-section TEM images for (b) sample 1 and (c) sample 11, both annealed for 20 s at 1020 °C, with α-Ge layers of 2.3 and 2.7 nm, respectively. (d) Cross-section TEM image of sample 12 after annealing for 600 s at 750 °C (d_0 =8.4 nm).

the NCs are found to depend strongly on the initial layer thickness. Figures 4(b) and 4(c) show typical NCs obtained after annealing sample 1 ($d_0=2.3$ nm) and sample 11 (d_0 =2.7 nm) for 20 s at 1020 °C. While the NCs in sample 11 extend almost over the whole layer stack, the NCs in sample 1 are much smaller. For an initial layer thickness of 8.4 nm (sample 12), a recrystallization of the continuous Ge layer was observed rather than a transformation into NCs with $r_{\mathrm{nc}} > d_0/2$ after annealing at 750 °C for 600 s [Fig. 4(d)].

The frequency distribution of NC radii, $\nu(r_{\mathrm{nc}})$, was analyzed for different initial Ge layer thicknesses d_0, as shown in Fig. 5. It was found that the shape of $\nu(r_{\mathrm{nc}})$ strongly depends on d_0. After 20 s annealing of sample 1 with d_0 =2.3 nm, a bimodal size distribution is obtained, as shown in Fig. 5(a). For sample 7 with $d_0=2.5$ nm, the first peak in $\nu(r_{\mathrm{nc}})$ almost disappears after 20 s annealing [Fig. 5(b)]. For the same initial layer thickness, however, a bimodal size distribution can still be observed for shorter annealing times, as shown in Fig. 5(b) for a 10 s annealing of sample 8. For the larger thickness $d_0=2.7$ nm (sample 10), no clear bimodal size distribution is observed already after 5 s annealing [Fig. 5(c)].

In the following, we suggest a simple thermodynamic model to explain the experimental findings. The model provides a quantitative explanation of the fundamental question why the continuous initial layer of α-Ge is transformed into isolated nanocrystals rather than exhibiting a simple recrystallization. This model is based on two fundamental concepts:

(1) the quasi-interface concept;[16]

(2) relaxation of the Ge/SiO_2 interface energy by structural adaptation.

The quasi-interface concept was introduced by Zacharias and Streitenberger[16] to explain the increase in recrystallization temperature T_c in α-Si/SiO_2 and α-Ge/SiO_2 superlattices. For an effective screening of the atomic interactions of

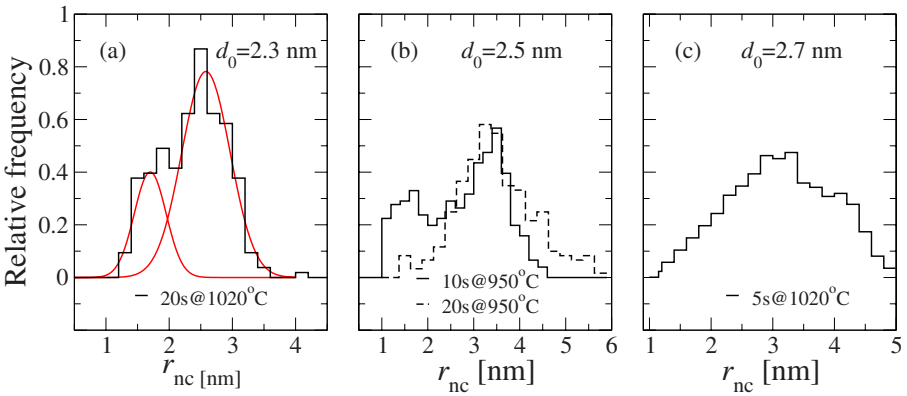

FIG. 5. (Color online) Normalized frequency distributions $\nu(r_{nc})$ of the NC radii for (a) sample 1, (b) samples 7 and 8, and (c) sample 10. In (a), the deconvolution of $\nu(r_{nc})$ into two Gaussian peak approximations is illustrated.

two phases, A and B, the thickness of a thin intermediate layer of phase C embedded between A and B has to be larger than a certain screening length. For a thermodynamic continuum description of intermediate layer thicknesses in the range of a few lattice constants, i.e., in the range of this screening length, one cannot attribute fixed specific energy values to the interfaces between A/C and C/B. Rather, the microscopic interactions between A and B can be taken into account by assuming a dependence of the interfacial energies for the A/C and C/B interfaces on the thickness of intermediate layer C. By this approach, the exponential increase in T_c with decreasing initial layer thickness d_0 was reproduced.[16] Analogous to the work of Zacharias and Streitenberger,[16] we assume the effective specific interface energy of the α-Ge/SiO_2 interface depending on the α-Ge layer thickness a as

$$\gamma_{o\alpha}^{\text{eff}}(a) = \gamma_{o\alpha}\left[1 - \exp\left(-\frac{a}{l_\alpha}\right)\right], \tag{5}$$

and the effective specific interface energy of the α-Ge/c-Ge interface as

$$\gamma_{\alpha c}^{\text{eff}}(a) = \gamma_{\alpha c} + (\gamma_{oc} - \gamma_{\alpha c})\exp\left(-\frac{a}{l_\alpha}\right). \tag{6}$$

Here, $\gamma_{o\alpha}$, $\gamma_{\alpha c}$, and γ_{oc} are the specific interface energies of an undisturbed α-Ge/SiO_2 interface, an undisturbed α-Ge/c-Ge interface, and an undisturbed c-Ge/SiO_2 interface, respectively. The parameter l_α can be considered as an effective screening length characteristic of amorphous Ge. The exponential dependence of the specific interface energies on the α-Ge layer thickness a is discussed in detail in the work of Zacharias and Streitenberger.[16]

For the section $s1$ of the initial α-Ge layer, as illustrated in Fig. 6(a), Eq. (5) yields a total interface energy of $2\gamma_{o\alpha}^{\text{eff}}(d/2)A_{o\alpha}^{s1} = 2\gamma_{o\alpha}A_{o\alpha}^{s1}$ in the limit of very large $d(d\to\infty)$. For $d\to 0$, i.e., for a vanishing initial layer, the total interface energy of section $s1$ also vanishes. For the section $s2$ of the nanocluster/matrix boundary [Fig. 6(a)], the total interface energy is $\gamma_{\alpha c}^{\text{eff}}(a_0)A_{\alpha c}^{s2} + \gamma_{o\alpha}^{\text{eff}}(a_0)A_{o\alpha}^{s2} = \gamma_{\alpha c}A_1^{s2} + \gamma_{o\alpha}A_2^{s2}$ for a very thick intermediate layer of amorphous Ge $(a_0\to\infty)$. For a vanishing intermediate layer of α-Ge, i.e., for $a_0\to 0$, Eqs. (5) and (6) yield a total interface energy of $\gamma_{oc}A_1^{s2}$. The exponential interpolation between these limiting cases ensures that the effective specific interface energies $\gamma_{o\alpha}^{\text{eff}}$ and $\gamma_{\alpha c}^{\text{eff}}$ only differ significantly from the respective undisturbed values when the thickness of the intermediate α-Ge layer is in the range of the screening length l_α.

It is known that the c-Ge/SiO_2 interface exhibits a relatively large interface energy.[16,29] There are two possible mechanisms for an interface energy relaxation: either a short-range adaptation of the oxide structure or a structural adaptation of the first monolayers of the Ge. While the first mechanism plays a role for the c-Si/SiO_2 interface,[30] the second mechanism seems more likely to us to explain the situation for the Ge/SiO_2 system. In our samples, the interface between the nanocrystal and the SiO_2 matrix is in contact with a reservoir of α-Ge, i.e., with the initial amorphous Ge layer surrounding the NC. For the specific interface energy values given below, a wetting of the nanocrystal surface by α-Ge is predicted since a c-Ge/SiO_2 interface would exhibit a larger interface energy. At the point of transition from the NC growth within the initial Ge layer to the outgrowth from it, we indeed observe such an intermediate layer of amorphous Ge, which separates the crystal from the top and bottom SiO_2 [Fig. 4(a)]. Thus we assume that the outgrowth of the NC from the initial layer is accompanied by the formation of such an α-Ge intermediate layer between the nanocrystal and the SiO_2 matrix. While the Ge contained in the amorphous interface layer is continuously incorporated into the nanocrystal, the material required to maintain the intermediate α-Ge layer for an increasing NC radius is continuously resupplied from the amorphous initial layer surrounding the NC.

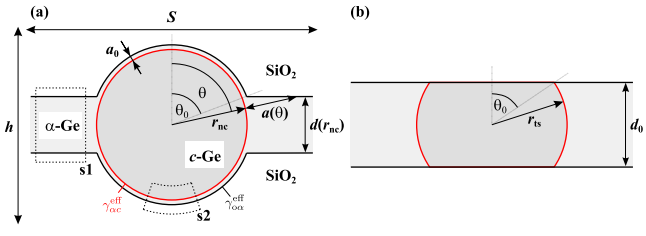

FIG. 6. (Color online) (a) Simplified cross-sectional geometries of the model for NC formation and for growth exclusively restricted to the (b) initial layer.

Based on these two basic concepts, we define a simple thermodynamic model as follows. Consider a cylindrical volume element V of arbitrary height $h \gg d_0$ enclosing a circular area of the layer stack corresponding to the mean capture area $\pi S^2/4$ of the nanocrystals [Fig. 6(a)]. S denotes the mean distance between the NC centers (Sec. III C). The constraints of our model are:

(a) fixed nanocrystal areal density, corresponding to a fixed value of S (Ref. 31);

(b) spherical shape of the NCs;

(c) periodical lateral boundary conditions due to neighboring NCs;

(d) neglect of the small difference in the bulk α-Ge and c-Ge densities;

(e) conservation of the total Ge and SiO_2 volume included in V; and

(f) disregard of strain effects[16,32] and of a roughening of the top SiO_2 surface due to a adaptation of the SiO_2 matrix to the Ge structure.[33]

The parameters required by the model are the undisturbed specific interfacial free energies $\gamma_{\alpha c}$, $\gamma_{o\alpha}$, and γ_{oc}, the difference in Gibbs free energies per unit volume of the amorphous and the crystalline Ge phase ΔG_v, and the intercluster distance S and the screening length l_α. As a reasonable approximation for the specific interface free energy $\gamma_{\alpha c}$ between the amorphous and the crystalline Ge phases, we use the value of the specific interface free energy $\gamma_{LS}=0.28\ \mathrm{J/m^2}$ of the interface between liquid and solid Ge.[24] Analogously, the specific interface energy $\gamma_{o\alpha}$ between the SiO_2 and the amorphous Ge phase is approximated by the specific interface free energy $\gamma_{oL}=0.7\ \mathrm{J/m^2}$ between SiO_2 and liquid Ge.[34] The interface energy $\gamma_{oc}=1.14\ \mathrm{J/m^2}$ between the c-Ge and the SiO_2 was obtained from the relation $\gamma_{oc}-\gamma_{o\alpha}=1.57\gamma_{\alpha c}$, as deduced by Zacharias and Streitenberger.[16] These parameters predict a wetting of the c-Ge in contact with the SiO_2 with amorphous Ge, i.e., the formation of an α-Ge intermediate layer, since $\gamma_{o\alpha}+\gamma_{\alpha c}<\gamma_{oc}$. The remaining parameter $\Delta G_v=G_{v\alpha}-G_{vc}>0$, i.e., the difference in Gibbs free energies per unit volume of the amorphous and the crystalline Ge phase, can be estimated to be $\Delta G_v=1.47\cdot 10^9\ \mathrm{J/m^3}$ from our experimental data as shown below. A constant value of the mean distance between the crystal nuclei $S=13$ nm is assumed representing a typical experimental result[31] (see Sec. III C). The most important parameter for our model is the effective screening length l_α for amorphous Ge. In the following, l_α is assumed to correspond to two Ge-Ge bond lengths $a_{\mathrm{GeGe}}=0.244$ nm (Ref. 35) giving the value of $l_\alpha=2\cdot a_{\mathrm{GeGe}}=0.488$ nm, which is similar to the value of $l_\alpha=0.63$ nm supposed by Zacharias and Streitenberger.[16]

The change $\Delta G^{\mathrm{NC}}(r_{\mathrm{nc}})$ in Gibbs free energy accompanying the formation of a spherical NC with radius r_{nc}, as compared to the case of no NC formation, can be shown to be given by Eq. (7). The derivation of this equation is based on simple geometrical arguments using volume and specific interface free energy densities of the different materials and phases. It is given in the Appendix.

$$\Delta G^{\mathrm{NC}}(r_{\mathrm{nc}}) = \Delta G^{\mathrm{volume,NC}} + \Delta G^{\mathrm{interface,NC}} + \Delta G^{\mathrm{interface,INITIAL}}. \tag{7}$$

Here, $\Delta G^{\mathrm{volume}}<0$ describes the energy release by the amorphous to crystalline phase transition of the Ge. The creation of an interface between the c-Ge and its environment during the growth of the NC gives a positive contribution to ΔG^{NC}. It is described by the second term in Eq. (7), which also includes the contribution of the interface between the intermediate α-Ge layer and the SiO_2. The third term in Eq. (7) denotes the change in the free energy of the interface between the remaining initial α-Ge layer and the SiO_2 due to a decreasing initial layer thickness during the NC growth [Eq. (5)]. All terms are given in the Appendix. The thickness $d(r_{\mathrm{nc}})$ of the remaining α-Ge initial layer can be calculated assuming conservation of the total Ge volume (Appendix).

As mentioned above, the intermediate α-Ge layer between the NC and the SiO_2 is formed to reduce the interface energy between the c-Ge and its environment (α-Ge, SiO_2). Therefore, its thickness a_0 has to be in the range of the screening length l_α (or larger) for an effective screening of the c-Ge/SiO_2 interactions [Eq. (6)]. One the other hand, for a given NC radius r_{nc}, the area of the interface between the intermediate α-Ge layer and the SiO_2 increases with increasing a_0, yielding a larger total interface energy $\Delta G^{\mathrm{interface,NC}}$. Therefore, there is an optimum intermediate layer thickness $a_0^\star > \max(d/2-r_{\mathrm{nc}},0)$ given by

$$\left.\frac{\partial \Delta G^{\mathrm{interface,NC}}(r_{\mathrm{nc}},a_0)}{\partial a_0}\right|_{r_{\mathrm{nc}}} = 0. \tag{8}$$

We assume that for each NC radius r_{nc}, the system can minimize the total interface energy by adapting the intermediate α-Ge layer thickness to $a_0^\star(r_{\mathrm{nc}})$. This assumption presupposes that the Ge diffusion processes necessary for the adaptation of the intermediate layer are faster than the NC growth itself, i.e., faster than the incorporation processes of Ge into the nanocrystal. Indeed, our results of the investigation of the NC ripening regime (Sec. III C) seem to support this picture since we found the ripening processes not to be limited by diffusion.

For the numerical solution of Eq. (7), we use the following algorithm:

(1) incrementation of the NC radius to $r_{\mathrm{nc},i}$;

(2) calculation of the optimal thickness $a_{0,i}^\star(r_{\mathrm{nc},i})$ for this NC radius using Eq. (8). If $\Delta G^{\mathrm{interface,NC}}$ does not exhibit a minimum, i.e., the formation of an intermediate α-Ge layer would not yield any energetical benefit for this NC radius, $a_{0,i}^\star$ is set to zero.

(3) Calculation of $\Delta G_i^{\mathrm{NC}}(r_{\mathrm{nc},i},a_{0,i}^\star)$ according to Eq. (7).

Besides the transformation of the initial layer into isolated NCs, an alternative pathway for the system considered would be a simple recrystallization of the continuous Ge layer. For this case, it is necessary to assume that no amorphous intermediate layer between the c-Ge and the SiO_2 is formed. Otherwise, the α-Ge contained in this intermediate layer would be continuously incorporated into the crystal, and the endeavor of the system to maintain the intermediate layer by a supply of α-Ge from the initial layer would yield an out-

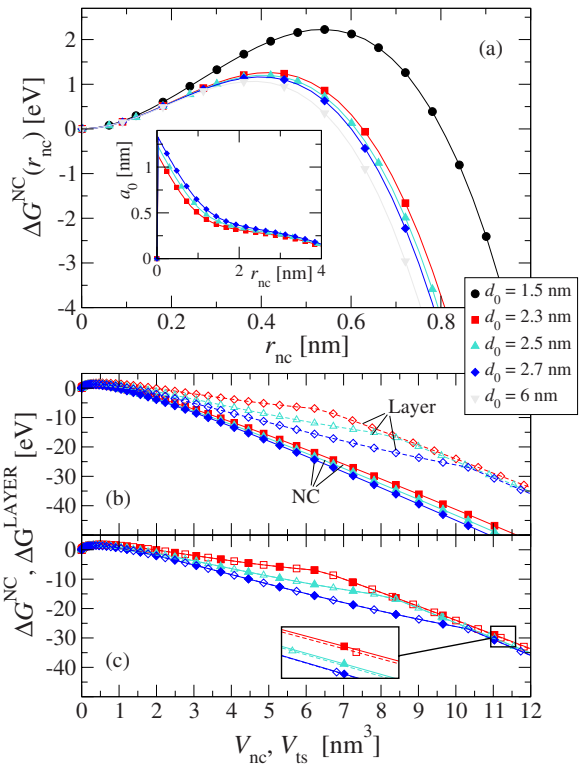

FIG. 7. (Color online) (a) Change in Gibbs free energies ΔG^{NC} for different thicknesses d_0 of the initial Ge layer as a function of crystal radius r_{nc}. The inset shows the optimal intermediate layer thickness $a_0^\star$ for d_0=2.3, 2.5, and 2.7 nm. (b) Comparison of ΔG^{NC} (filled symbols) and $\Delta G^{\mathrm{LAYER}}$ (open symbols) for the same c-Ge volume V_{NC} and V_{ts}, respectively. (c) Comparison of ΔG^{NC} and $\Delta G^{\mathrm{LAYER}}$ for the case of an absence of a relaxation of the Ge/SiO_2 interface energy by a formation of an intermediate α-Ge layer between the NC and the SiO_2. The inset shows an enlarged view of the region 11 nm$\leq V_{\mathrm{NC}}, V_{\mathrm{ts}} \leq$ 12 nm.

growth of the crystal into the SiO_2. The restriction of the crystal growth to the initial layer can by described by assuming truncated sphere shapes for crystal nuclei with $r_{\mathrm{ts}} > d_0/2$ [Fig. 6(b)]. Then the limit $r_{\mathrm{ts}} \rightarrow S/2$ corresponds to a complete recrystallization of the continuous Ge layer. The change in Gibbs free energy $\Delta G^{\mathrm{layer}}(r_{\mathrm{ts}})$ for the growth of a crystal nucleus with $r_{\mathrm{ts}} > d_0/2$ according to this pathway is given by

$$\Delta G^{\mathrm{LAYER}}(r_{\mathrm{ts}}) = \Delta G^{\mathrm{volume,TS}} + \Delta G^{\mathrm{interface,TS}}. \tag{9}$$

Again, both terms are given in the Appendix. In contrast to Eq. (7), the third term describing the change in the free energy of the interface between the remaining initial α-Ge layer and the SiO_2 due to a decreasing initial layer thickness is not present in Eq. (9) since the initial layer thickness is not altered during crystal growth.

Figure 7(a) shows the simulated behavior of $\Delta G^{\mathrm{NC}}(r_{\mathrm{nc}})$ for different initial layer thicknesses d_0. As known from classical nucleation theory,[27] the free energy increases in the initial stage of nucleation until the crystal reaches a critical size $r_{\mathrm{nc1}}^\star$. This is due to the creation of an interface between the crystalline and the amorphous Ge phase. For $r_{\mathrm{nc}} > r_{\mathrm{nc1}}^\star$ this increase in ΔG^{NC} is overcompensated by the energy released by the amorphous to crystalline phase transition so that nuclei with a radius larger than $r_{\mathrm{nc1}}^\star$ are stable and can grow further in size. The energy barrier $\Delta G_1^* = \Delta G^{\mathrm{NC}}(r_{\mathrm{nc1}}^\star)$ corresponds to the nucleation energy to form a stable nucleus. Obviously, the height of ΔG_1 as well as the critical NC radius $r_{\mathrm{nc1}}^\star$ depend on the initial layer thickness d_0. This dependence is stronger for smaller d_0, while there is a saturation value of ΔG_1^* for large values of d_0 corresponding to the nucleation energy of bulk Ge. The increase in ΔG_1^* with decreasing d_0 is a consequence of the quasi-interface concept and yields an exponential increase in the recrystallization temperature with decreasing initial layer thickness.[16] The reasons for this effect are the increasing interatomic interactions between the oxide and the c-Ge, yielding an increasing effective interface energy of the NC. In the limit of $d_0/2 \gg l_\alpha$, the nucleation energy can be calculated by classical nucleation theory as follows:[27]

$$\Delta G_1^* = \frac{16}{3}\pi \frac{\gamma_{\alpha c}^3}{\Delta G_v^2}. \tag{10}$$

One should note that it is not possible to calculated ΔG_v directly from Eq. (10) using our experimental extracted value of ΔG_1^* (Fig. 3) and the literature value of $\gamma_{\alpha c}$,[24] which would yield $\tilde{G}_v = 1.38 \cdot 10^9$ J/m^3. Rather, the value of $\Delta G_1^* = 1.2$ eV was extracted from samples with d_0=2.5 nm and d_0=2.7 nm. As shown in Fig. 7(a), the nucleation energies for these two values of d_0 do not significantly differ from each other but are increased as compared to the case of large initial layer thicknesses. Therefore, ΔG_v was adapted in order to reproduce a nucleation energy of ΔG_1^*=1.2 eV for d_0=2.5 nm by the model, yielding a value of $\Delta G_v = 1.47 \cdot 10^9$ J/m^3. In agreement with our experimental observations, a further decrease in d_0 down to 2.3 nm yields a significant increase in the nucleation energy. For $d_0 = 1.5$ nm, ΔG_1^* is increased by a factor of $\approx$2 as compared to the bulk value. We expect that for initial layer thicknesses in this range, homogeneous nucleation within the initial layer is extremely unlikely also for higher annealing temperatures than used in our experiments. A minimum initial layer thickness $d_0^{\mathrm{min}} \approx 1.5$ nm for the observation of recrystallization is also reported by Williams *et al.*[28] and Zacharias and Streitenberger.[16] Regarding the critical NC radius $r_{\mathrm{nc1}}^\star$, we obtain $r_{\mathrm{nc1}}^\star = 2\gamma_{\alpha c}/\Delta G_v = 0.38$ nm for the limit $d_0/2 \gg l_\alpha$ from classical nucleation theory. For d_0=2.5 nm, the critical NC radius is increased to 0.42 nm. These values are smaller than the value of $r_{\mathrm{nc1}}^\star$=1 nm obtained by molecular dynamics simulations.[36] However, a NC with a critical radius of 1 nm would almost reach the SiO_2 in our systems investigated, yielding a huge increase in the nucleation energy due to the c-Ge/SiO_2 interactions. Therefore, we believe that our extracted values of $r_{\mathrm{nc1}}^\star \leq 0.5$ nm are more plausible.

The inset of Fig. 7(a) shows the optimal thickness $a_0^\star$ of the intermediate α-Ge layer formed between the NC and the oxide in order to relax the interface energy of the NC. Already for $r_{\mathrm{nc}} < d_0/2$, $a_0^\star$ is slightly larger than $d_0/2 - r_{\mathrm{nc}}$; i.e., the structural adaptation of the α-Ge between the NC and the oxide yields an energetic benefit even if the NC size does not

exceed the initial layer thickness yet. For $r_{nc} > d_0/2$, $a_0^\star$ exhibits a plateau value almost independent of d_0. This value is mainly determined by l_α since a larger intermediate layer thickness would not yield a more effective screening of the c-Ge/SiO_2 interactions but would increase the effective NC interface area. The latter effect is also the reason why the intermediate layer thickness $a_0^\star$ is decreasing for increasing r_{nc}. This observation explains the absence of an intermediate layer in our TEM images for larger nanocrystals. In Fig. 7(b), the change in the free energy for the case of a formation of a spherical nanocrystal growing out of the initial layer with $r_{nc} > d_0/2$ according to Eq. (7) is compared with the case of a growth restricted to the initial layer [Eq. (9)] for d_0=2.3, 2.5 and 2.7 nm. Especially within the crucial range of $V_{NC} \sim 4/3\pi(d_0/2)^3$, i.e., at the transition point when the NC size reaches the initial layer thickness, the absolute value of ΔG^{LAYER} is always smaller than the corresponding ΔG^{NC} value. This means that the total free energy of the system is larger for a simple recrystallization of the continuous layer than for the formation of isolated NCs with $r_{nc} > d_0/2$. In this regime of V_{NC}, the energetic benefit of the outgrowth from the initial layer is essentially based on the relaxation of the NC interface energy by the formation of the intermediate α-Ge layer. In Fig. 7(c), ΔG^{NC} is shown for the case of an absence of the Ge/SiO_2 interface energy relaxation, i.e., without a formation of an intermediate layer ($a_0^\star = 0 \forall r_{nc}$). In this case, the outgrowth from the initial layer would be energetically unfavorable compared to the case of a further growth within the initial layer. Therefore, the separation of the c-Ge from the SiO_2 by an intermediate α-Ge layer is essential to explain the transformation of the continuous initial layer of α-Ge into isolated NCs. For increasing initial layer thickness, one expects an upper limit $d_0 = d_0^{max}$ for NC formation rather than a recrystallization of the continuous layer. While this limit is expected to depend on the annealing parameters, we observe a recrystallization of the continuous layer for d_0=8.4 nm after annealing for 600 s at 750 °C [Fig. 4(d)]. This transition from NC formation to a continuous recrystallization can be explained by the amount of α-Ge available for each crystal nucleus. Since the probability per unit time for the formation of a stable nucleus scales with the α-Ge volume of the initial layer, the areal density of nuclei can be expected to increase with increasing initial layer thickness [Eq. (4)]. If the nuclei are formed very close to each other, the remaining α-Ge in between will not be sufficient for an outgrowth from the initial layer. In particular, no α-Ge intermediate layer between the c-Ge and the SiO_2 can be formed when neighboring crystals reach almost simultaneously the interface to the bottom and top SiO_2.

So far, the model does not explain the shape of the observed NC size distributions $\nu(r_{nc})$. Especially, the bimodal frequency distribution of the NC radii in some of our samples is puzzling.

We conjecture that this observation could be attributed to the existence of a second barrier ΔG_2^* in the actual $\Delta G^{NC}(r_{nc})$ which appears at a critical radius $r_{nc2}^\star > r_{nc1}^\star$ due to an effect that has not been included in our model (Fig. 8). In this picture, the first peak of the bimodal size distribution can be attributed to NCs that have overcome the first energy barrier ΔG_1^* but not the second barrier ΔG_2^*. Their size should

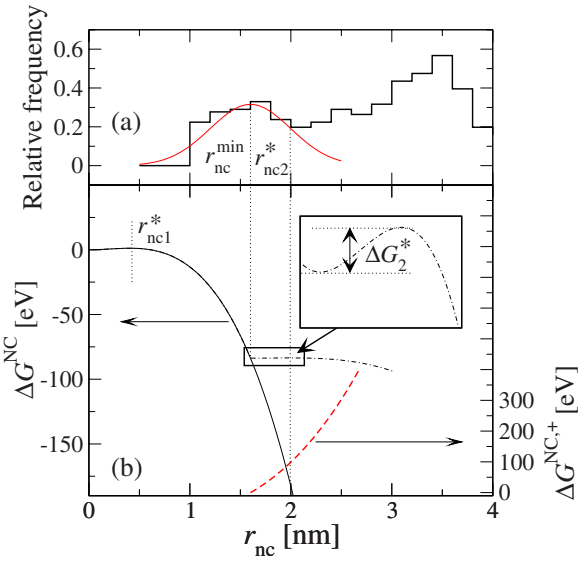

FIG. 8. (Color online) (a) Relative frequency distribution $\nu(r_{nc})$ of the NC radii of sample 7 with d_0=2.5 nm. (b) Simulated change in the free energy during NC growth for d_0=2.5 nm (solid line). The inset shows an enlarged view of the assumed second barrier ΔG_2^* deduced from the bimodal shape of $\nu(r_{nc})$. The dependence of the additional contribution $\Delta G^{NC,+}$ on the NC radius (dashed line), as well as the total change in the free energy $\Delta G^{NC} + \Delta G^{NC,+}$ (dashed-dotted line), was estimated from the position and the value of the local maximum and minimum, respectively, by using a simple functional analysis.

roughly correspond to the radius r_{nc}^{min} of the local minimum in $\Delta G^{NC}(r_{nc})$ between the two barriers [Fig. 8(a)]. The second peak corresponds to NCs that have overcome both barriers. With increasing annealing time, the probability that a nucleus also overcomes the second barrier ΔG_2^* is increasing. Therefore, the first peak in $\nu(r_{nc})$ vanishes and no bimodal size distribution occurs for longer annealing times [Fig. 5(b)].

In the following, we estimate the height of this hypothetical second barrier ΔG_2^* that would be required to explain the experimental results. The probability p_1 per unit time that a crystal nucleus overcomes the first energy barrier ΔG_1^* is given by $p_1 \propto \exp(-\Delta G_1^*/k_B T)$.[27] Once the first barrier is surpassed, the probability p_2 per unit time that a nucleus overcomes the second barrier is given by $p_2 \propto \exp(-\Delta G_2^*/k_B T)$.

The relative number of NCs belonging to the first peak is represented by its area a_1 in the normalized size distribution $\nu(r_{nc})$ [Fig. 5(a)]. It can be linked to the probability that a nucleus overcomes the first but not the second barrier within a given annealing time t. Analogously, the relative number of NCs corresponding to the area a_2 of the second peak in $\nu(r_{nc})$ corresponds to the probability that both barriers are overcome during this time. Therefore the following proportionalities should hold:

$$a_1 \propto p_1 \bar{p}_2 = p_1(1 - p_2),$$

$$a_2 \propto p_1 p_2. \tag{11}$$

From these assumptions, it follows that the ratio of both peak areas depends only on p_2 and that it is determined by

$$\frac{a_1}{a_2}+1=\frac{1}{p_2}\propto\exp\left(\frac{\Delta G_2^*}{k_BT}\right). \tag{12}$$

This means that the energy barrier ΔG_2^* can be extracted from the experimentally observed temperature behavior of a_1/a_2+1 in annealing experiments of layers with a given initial thickness d_0. The peak areas a_1 and a_2 were determined by approximating $\nu(r_{nc})$ by the sum of two Gaussians as can be seen in the example of Fig. 5(a). An Arrhenius plot of a_1/a_2+1 for samples 5, 6, and 7 (not shown) yields $\Delta G_2^*=(0.1\pm0.05)$ eV for $d_0=2.5$ nm. It should be noted that this analysis is a rough estimation of the height of the assumed second barrier rather than an exact determination, which is limited by the number of data points.

Our model, however, predicts a monotonic decrease in $\Delta G^{NC}(r_{nc})$ for $r_{nc}>r_{nc1}^{\star}$ for all values of d_0 and no second barrier can be obtained by the model within its assumptions mentioned above. If our supposition is correct and a second barrier in the change of the free energy occurs in our samples during NC growth, it should be caused by a mechanism neglected so far. We suspect that the neglect of strain effects is the most questionable. It has been shown by Zacharias and Streitenberger[16] that the inhomogeneous strain during the recrystallization of amorphous Si layers increases exponentially with decreasing layer thickness. For our samples, the bimodal shape of the NC size distribution function $\nu(r_{nc})$ is more pronounced for samples with a small initial layer thickness. Therefore, the second barrier could be caused by strain effects occurring during the outgrowth of the NC and the structural adaptation of the SiO_2. For $d_0=2.5$ nm, the NC radius r_{nc}^{min} corresponding to the position of the first peak in $\nu(r_{nc})$, i.e., to the supposed local minimum in $\Delta G^{NC}(r_{nc})$ is 1.6 nm [Fig. 8(a)]. The position of the second barrier is expected to correspond to the local minimum in $\nu(r_{nc})$ at $r_{nc2}^{\star}=2$ nm. An additional positive contribution $\Delta G^{NC,+}$ of ≈100 eV to the $\Delta G^{NC}(r_{nc})$ of our model would be required in this range to overcompensate the decrease of ΔG^{NC} between r_{nc}^{min} and $r_{nc2}^{\star}$ in order to obtain a second barrier $\Delta G_2^*=\Delta G^{NC}(r_{nc2}^{\star})-\Delta G^{NC}(r_{nc}^{min})$ [Fig. 8(b)]. Such an additional contribution of $\Delta G^{NC,+}\approx100$ eV to the free energy would correspond to a pressure of ≈1 GPa for $V_{NC}(r_{nc}^{min})$. This value is on the same order of magnitude as the values reported by Sharp *et al.*[32] for ion beam synthesized Ge NCs in SiO_2. One can estimate the dependence of the additional contribution $\Delta G^{NC,+}$ on the NC radius from the position and the value of the local maximum and minimum, respectively, by a functional analysis assuming the lowest polynomial approximation. We found $\Delta G^{NC,+}$ to scale with r_{nc}^3, i.e., with the volume of the nanocrystal [Fig. 8(b)]. This supports the assumption that strain effects may be the reason for the second barrier. However, we expect that the strain energy be stored in the system by inelastic rather than elastic deformation, since Ge NCs embedded in SiO_2 are known to exhibit stress relaxation during thermal annealing.[32] Furthermore, as we do not observe a roughening of the top SiO_2 surface even after the formation of larger NCs, we assume that the energy corresponding to the second barrier is dissipated in the SiO_2 during the outgrowth of the nanocrystals.

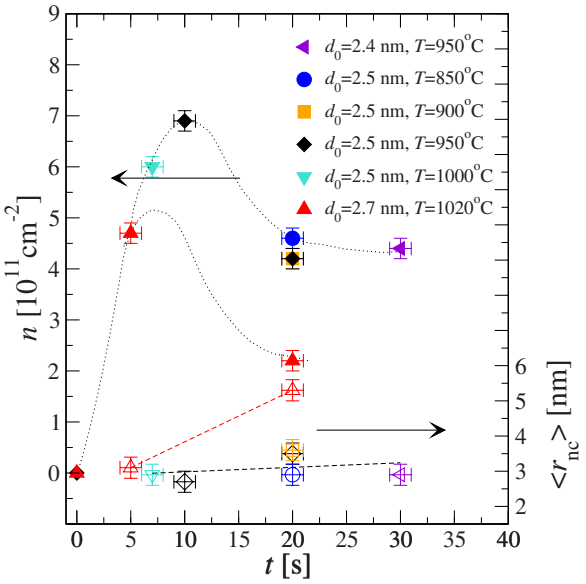

FIG. 9. (Color online) Nanocrystal areal density n (full symbols) and mean NC radius $\langle r_{nc}\rangle$ (open symbols) as a function of annealing time for different annealing temperatures and initial layer thicknesses. The lines are a guide for the eyes.

C. Ripening of the nanocrystals (stage 3)

As mentioned above, we observe ripening phenomena for longer annealing times. In this regime, the NC areal density n is decreasing with increasing t while the mean NC radius $\langle r_{nc}\rangle$ increases [Fig. 9]. The transition from the stage of NC outgrowth to the ripening regime is floating and depends on the annealing temperature. For higher temperatures, it occurs at an earlier point in time.

Ostwald ripening effects, i.e., the growth of larger NCs at the expense of smaller ones, can be observed in SEM planview images of samples where the top oxide was removed by wet chemical etching after NC formation [Fig. 10(a)]. Due to the different secondary electron yields of Ge and SiO_2,[37,38]

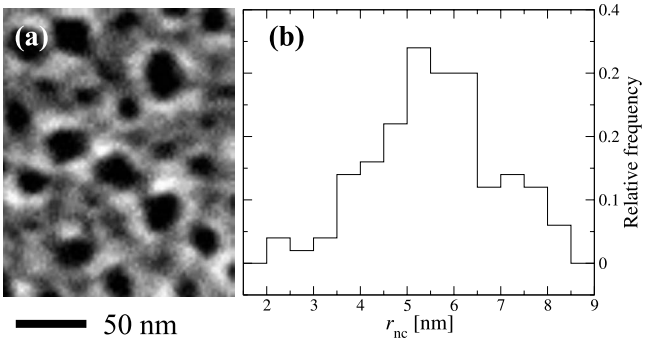

FIG. 10. (a) SEM planview image of sample 11, showing that only large NCs (dark) are surrounded by an area of low Ge concentration (bright regions, see text). The top oxide was removed by HF etching after NC formation. Note that the NCs are slightly smaller than the reliable SEM resolution. (b) Normalized frequency distribution $\nu(r_{nc})$ of the NC radii for sample 11. These data were obtained by TEM and are therefore much more accurate than the apparent NC sizes shown in (a).

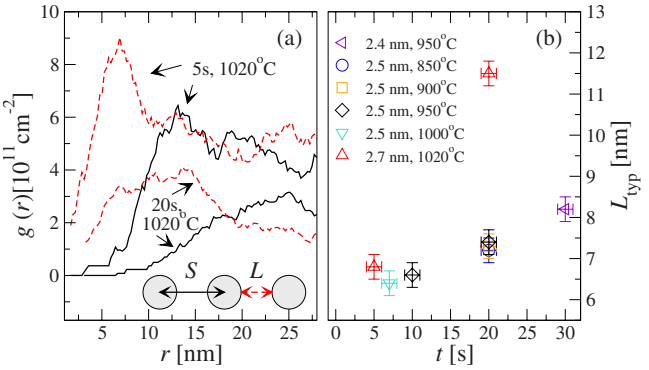

FIG. 11. (Color online) (a) Radial distribution function $g(r)$ of the intercluster distance L and the distance S between the cluster centers for samples 10 and 11. (b) Typical intercluster distance L_{typ} as a function of annealing time for different annealing temperatures and initial layer thicknesses.

Ge enriched areas appear dark, while areas of Ge depletion appear brighter. Obviously, only the larger NCs are surrounded a by a bright circular ring, corresponding to an area of Ge depletion compared to the Ge concentration of the environment. The smaller NCs do not exhibit this feature. This observation indicates that the larger NCs attract Ge from the environment during further growth, while the smaller NCs shrink and dispense Ge to the environment. The corresponding frequency distribution of r_{nc} for sample 11 is shown in Fig. 10(b). This distribution is broad and unsymmetrical. However, from the shape of this distribution, it is not possible to clearly distinguish whether the ripening is limited by diffusion or by reaction rate. There are several reasons for the deviation of the observed shape of $\nu(r_{\mathrm{nc}})$ from those predicted by theoretical models for Ostwald ripening, e.g., the one of Lifshitz and Slyozow[39] and Wagner.[39] In contrast to their basic assumptions, additional NCs can be formed by nucleation during the ripening process, since the transition from stages 1 and 2 to stage 3 is floating and occurs at a point in time where a large amount of the initial layer is not yet transformed into crystalline NCs. Furthermore, the total volume of the NCs is very large, and the concentration of Ge is spatially inhomogeneous.

To obtain further insight into the mechanisms of the ripening process, we have analyzed the intercluster distances $L(t,T,d_0)$. For Ge enriched SiO_2 prepared by cosputtering of SiO_2 and Ge, Takeoka *et al.*[11] reported the intercluster distance L to be determined by the diffusion length of Ge in SiO_2. This picture was adapted to the growth of Si NCs in SiO_2 by Riabinina *et al.*[40] In order to analyze the dependence of $L(t,T,d_0)$ on annealing time, temperature, and initial layer thickness d_0, we determined the radial areal frequency distribution $g(r)$ for the intercluster distances L and the distances S between the NC centers. The distribution function $g(r)$ describes the probability $g(r)2\pi r\Delta r$ to find neighboring crystals within a radius interval $(r,r+\Delta r)$ [Fig. 11(a)]. It was obtained by determining the number of neighboring NCs within a distance $(r,r+\Delta r)$ for each nanocrystal, normalizing to $2\pi r\Delta r$ (corrected for edge effects), and averaging over all NCs.

Figure 11(a) demonstrates that this areal distribution of the NCs is not random. Rather, $g(r)$ exhibits a significant peak, which can be attributed to a typical distance between a NC and its nearest neighbors. The peak positions are denoted by L_{typ} and S_{typ}, respectively (see Table I). The value of $(\pi S_{\mathrm{typ}}^2/4)^{-1}$ roughly corresponds to the mean areal density n of the NCs. Figure 11(b) shows the dependence of L_{typ} on the annealing time for different T and d_0. With in increasing annealing time, L_{typ} increases. Surprisingly, the dependence on the annealing temperature is very weak. All samples with the same d_0, annealed for the same time t, exhibit almost the same intercluster distance L regardless of the annealing temperature. This observation contradicts the assumption that L is determined by a Ge diffusion length. Regardless of whether the Ge diffusion mainly takes place within the initial Ge layer, along the Ge/SiO_2 interface or within the SiO_2, the diffusion constant should be thermally activated, which would yield a much stronger temperature dependence of L. We therefore believe that the ripening process is not limited by diffusion in our samples. The reason for the opposite findings of Takeoka *et al.*[11] may be seen in the fact that in our samples there is a high Ge concentration ($\approx$100%) within the amorphous Ge layer, which provides sufficient material for the ripening process. The rather fast diffusion processes support our assumption that the thickness of the intermediate α-Ge layer between the c-Ge and the SiO_2 can be adjusted to the optimum value $a_0^\star$ corresponding to a minimal NC interface energy for each NC radius (Sec. III B).

IV. CONCLUSION

In summary, we have analyzed quantitatively the driving forces of the transformation of an ultrathin continuous layer of elementary Ge embedded in SiO_2 into isolated NCs. The influence of annealing time, temperature, and layer thickness on the NC formation was studied by detailed TEM investigations. In general, the NC formation process was found to exhibit three different subsequent stages: In the first stage, NCs grow within the layer by homogeneous nucleation. During the second stage, the crystal size exceeds the layer thickness, and the crystals grow into the SiO_2. This process can be explained by the formation of an intermediate layer of amorphous Ge between the nanocrystal and the SiO_2, which provides the material required for the outgrowth and which minimizes the Ge/SiO_2 interface energy. Therefore, this pathway is energetically preferred to a simple recrystallization of the layer. A simple thermodynamic model essentially based on the quasi-interface concept and on Ge/SiO_2 interface energy relaxation reproduces quantitatively these experimental findings. The bimodal nanocrystal size distribution observed under certain conditions can tentatively be explained by the existence of a second barrier in the Gibbs free energy. The additional positive contribution to the free energy necessary to form this second barrier may arise from inelastic strain effects occurring during the outgrowth of the NC from the initial layer. The third stage is a ripening process of the clusters, which seems not to be limited by diffusion. We hope that our results provide stimulations for further experimental and theoretical (e.g., molecular dynamics) investigations.

ACKNOWLEDGMENTS

This work was funded by Deutsche Forschungsgemeinschaft under Grant No. HO 1885/8-2.

APPENDIX: CHANGE IN GIBBS FREE ENERGY

In the absence of any crystal nucleus in the amorphous Ge layer, the Gibbs free energy of a volume element considered (Fig. 6) is given by

$$G_0 = d_0\pi\frac{S^2}{4}G_{v\alpha} + V_{\mathrm{ox}}G_{\mathrm{vo}} + 2\pi\frac{S^2}{4}\gamma_{o\alpha}^{\mathrm{eff}}(d_0/2). \quad \text{(A1)}$$

The first and the second terms are related to the amorphous Ge and the SiO_2 bulk volume, respectively. The third term is the contribution of the interface between the amorphous Ge phase and the oxide. $V_{\mathrm{ox}}=(h-d_0)\pi S^2/4$ is the volume of the SiO_2 included in the chosen element. In case of the formation of a nucleus, the free energy can be written as

$$\begin{aligned} G^{\mathrm{NC}}(r_{\mathrm{nc}},a_0^\star) &= \left(d_0\pi\frac{S^2}{4} - \frac{4}{3}\pi r_{\mathrm{nc}}^3\right)G_{v\alpha} + \frac{4}{3}\pi r_{\mathrm{nc}}^3 G_{vc} + V_{\mathrm{ox}}G_{\mathrm{vo}} \\ &+ 2\int_0^{2\pi}\int_{\Theta_0}^{\pi} r_{\mathrm{nc}}^2\sin(\Theta)\gamma_{\alpha c}^{\mathrm{eff}}[a(\Theta)]d\Theta d\varphi \\ &+ 2\int_0^{2\pi}\int_0^{\Theta_0} r_{\mathrm{nc}}^2\sin(\Theta)\gamma_{\alpha c}^{\mathrm{eff}}(a_0^\star)d\Theta d\varphi \\ &+ 2\int_0^{2\pi}\int_0^{\Theta_0} (r_{\mathrm{nc}}+a_0^\star)^2\sin(\Theta)\gamma_{o\alpha}^{\mathrm{eff}}(a_0^\star)d\Theta d\varphi \\ &+ 2\pi\left\{\frac{S^2}{4} - [\sin(\Theta_0)(r_{\mathrm{nc}}+a_0^\star)]^2\right\} \\ &\times\gamma_{o\alpha}^{\mathrm{eff}}[d(r_{\mathrm{nc}})/2]. \end{aligned} \quad \text{(A2)}$$

The first three terms are related to the α-Ge, c-Ge volume, and SiO_2 volume, respectively. The fourth term describes the contribution of the α-Ge/c-Ge interface within the initial layer. The angle Θ_0 is equal to $\arccos\{d(r_{\mathrm{nc}})/[2(r_{\mathrm{NM}}+a_0^\star)]\}$ for $a_0^\star+r_{\mathrm{nc}}>d_0/2$ and zero otherwise. For $\Theta>\Theta_0$, the radial distance $a(\Theta)$ from the NC boundary to the SiO_2 can be calculated by $a(\Theta)=d(r_{\mathrm{nc}})/(2\cos(\Theta))-r_{\mathrm{nc}}$. The fifth term in Eq. (A2) describes the interface between the NC and the intermediate α-Ge layer with a fixed thickness $a_0^\star$. The sixth term corresponds to the interface between the intermediate layer and the oxide. The seventh term describes the α-Ge/SiO_2 interface of the remaining initial α-Ge layer.

Assuming volume conservation, $\Delta G^{\mathrm{NC}}(r_{\mathrm{nc}})=G^{\mathrm{NC}}(r_{\mathrm{nc}})-G_0$ corresponding to Eq. (7) can be obtained by subtracting Eq. (A1) from Eq. (A2). The single terms are given by

$$\Delta G^{\mathrm{volume,NC}} = -\frac{4}{3}\pi r_{\mathrm{nc}}^3\Delta G_v,$$

$$\begin{aligned} \Delta G^{\mathrm{interface,NC}}(r_{\mathrm{nc}},a_0^\star) &= 2\int_0^{2\pi}\int_{\Theta_0}^{\pi} r_{\mathrm{nc}}^2\sin(\Theta)\gamma_{\alpha c}^{\mathrm{eff}}[a(\Theta)]d\Theta d\varphi \\ &+ 2\int_0^{2\pi}\int_0^{\Theta_0} r_{\mathrm{nc}}^2\sin(\Theta)\gamma_{\alpha c}^{\mathrm{eff}}(a_0^\star)d\Theta d\varphi \\ &+ 2\int_0^{2\pi}\int_0^{\Theta_0} (r_{\mathrm{nc}}+a_0^\star)^2\sin(\Theta)\gamma_{o\alpha}^{\mathrm{eff}}(a_0^\star)d\Theta d\varphi \\ &- 2\pi[\sin(\Theta_0)(r_{\mathrm{nc}}+a_0^\star)]^2\gamma_{o\alpha}^{\mathrm{eff}}(d_0/2), \end{aligned}$$

$$\begin{aligned} \Delta G^{\mathrm{interface,INITIAL}} &= 2\pi\left\{\frac{S^2}{4} - [\sin(\Theta_0)(r_{\mathrm{nc}}+a_0^\star)]^2\right\} \\ &\times\{\gamma_{o\alpha}^{\mathrm{eff}}[d(r_{\mathrm{nc}})/2] - \gamma_{o\alpha}^{\mathrm{eff}}(d_0/2)\}. \end{aligned}$$

For $r_{\mathrm{nc}}+a_0^\star>d_0/2$, the thickness of the remaining amorphous Ge layer, $d(r_{\mathrm{nc}},a_0^\star)$, is decreasing for increasing r_{nc} and increasing $a_0^\star$. It can be calculated considering conservation of the total Ge volume $V_{\mathrm{NC}}+V_{\mathrm{Ge}}^\alpha=V_{\mathrm{Ge}}^0$, yielding

$$\begin{aligned} \pi\frac{S^2}{4}[d_0-d(r_{\mathrm{nc}})] &= \frac{4}{3}\pi[r_{\mathrm{nc}}+a_0^\star(r_{\mathrm{nc}})]^3 + \frac{1}{12}\pi d^3(r_{\mathrm{nc}}) - \pi d(r_{\mathrm{nc}}) \\ &\times[r_{\mathrm{nc}}+a_0^\star(r_{\mathrm{nc}})]^2. \end{aligned}$$

For further growth exclusively within the initial layer, i.e., for a description of the crystals with $r_{\mathrm{ts}}>d_0/2$ by truncated spheres (tss) corresponding to Eq. (9), one obtains by an analogous derivation,

$$\Delta G^{\mathrm{volume,TS}} = \begin{cases} -\frac{4}{3}\pi r_{\mathrm{ts}}^3\Delta G_v & r_{\mathrm{ts}} \le d_0/2 \\ -\left\{\pi d_0[r_{\mathrm{ts}}\sin(\Theta_0)]^2 + \frac{\pi d_0^3}{6}\right\}\Delta G_v & \text{otherwise} \end{cases},$$

$$\begin{aligned} \Delta G^{\mathrm{interface,TS}}(r_{\mathrm{ts}}) &= 2\int_0^{2\pi}\int_{\Theta_0}^{\pi} r_{\mathrm{ts}}^2\sin(\Theta)\gamma_{\alpha c}^{\mathrm{eff}}[a(\Theta)]d\Theta d\varphi \\ &+ 2\pi[\sin(\Theta_0)r_{\mathrm{ts}}]^2[\gamma_{\mathrm{oc}} - \gamma_{o\alpha}^{\mathrm{eff}}(d_0/2)]. \end{aligned}$$

Here, Θ_0 is equal to $\arccos[d(r_{\mathrm{nc}})/(2r_{\mathrm{ts}})]$ for $r_{\mathrm{ts}}>d_0/2$ and zero otherwise.

*peibst@mbe.uni-hannover.de

[1] L. T. Canham, Appl. Phys. Lett. **57**, 1046 (1990).

[2] H. Takagi, H. Ogawa, Y. Yamazaki, A. Ishizaki, and T. Nakagiri, Appl. Phys. Lett. **56**, 2379 (1990).

[3] Y. Maeda, Phys. Rev. B **51**, 1658 (1995).

[4] S. Tiwari, F. Rana, H. Hanafi, E. F. Crabbe, and K. Chan, Appl. Phys. Lett. **68**, 1377 (1996).

[5] L. Pavesi, L. Dal Negro, C. Mazzoleni, G. Franzo, and F. Priolo, Nature (London) **408**, 440 (2000).

[6] D. Riabinina, C. Durand, M. Chaker, N. Rowell, and F. Rosei,

Nanotechnology **17**, 2152 (2006).
[7] A. Fissel, A. Laha, E. Bugiel, D. Khne, M. Czernohorsky, R. Dargis, and H. J. Osten, Microelectron. J. **39**, 512 (2008).
[8] J. Durfourcq, S. Bodnar, G. Gay, D. Lafond, P. Mur, G. Molas, J. P. Nieto, L. Vandroux, L. Jodin, F. Gustavo, and Th. Baron, Appl. Phys. Lett. **92**, 073102 (2008).
[9] H. Fukuda, S. Sakuma, S. Nomura, M. Nishino, T. Higuchi, and S. Ohshima, J. Appl. Phys. **90**, 3524 (2001).
[10] V. Beyer, J. v. Borany, and M. Klimenko, Appl. Phys. Lett. **89**, 193505 (2006).
[11] S. Takeoka, M. Fujii, S. Hayashi, and K. Yamamoto, Phys. Rev. B **58**, 7921 (1998).
[12] W. K. Choi, H. G. Chew, V. Ho, V. Ng, W. K. Chim, Y. W. Ho, and S. P. Ng, J. Cryst. Growth **288**, 79 (2006).
[13] S. Ăgan, A. Dana, and A. Aydinli, J. Phys.: Condens. Matter **18**, 5037 (2006).
[14] Y. C. King, T. J. King, and C. Hu, IEEE Trans. Electron Devices **48**, 696 (2001).
[15] A. Kanjilal, J. L. Hansen, P. Gaiduk, N. Larsen, P. Normand, E. Kapelanakis, D. Skarlatos, and D. Tsoukalas, Appl. Phys. Lett. **82**, 1212 (2003).
[16] M. Zacharias and P. Streitenberger, Phys. Rev. B **62**, 8391 (2000).
[17] G. F. Crom, D. J. Lockwood, J. P. McCaffey, H. J. Labbé, P. M. Fauchet, B. White, Jr., J. Diener, D. Kovalev, F. Koch, and L. Tybeskov, Nature (London) **407**, 358 (2000).
[18] C. L. Heng, W. W. Tjiu, and T. G. Finstad, Appl. Phys. A **A78**, 1181 (2004).
[19] C. L. Heng, Y. J. Liu, A. T. S. Wee, and T. G. Finstad, J. Cryst. Growth **262**, 95 (2004).
[20] T. Dürkop, E. Bugiel, I. Costina, A. Ott, R. Peibst, and K. R. Hofmann, Mater. Sci. Eng., B **147**, 213 (2008).
[21] H. Z. Massoud and J. D. Plummer, J. Appl. Phys. **62**, 3416 (1987).
[22] One should note that the sensitivity factors are only accurate for pure elements; therefore, the real concentration can slightly differ from the estimated one.
[23] D. C. Paine, C. Caragianis, and A. F. Schwartzmann, J. Appl. Phys. **70**, 5076 (1991).
[24] Q. Xu, I. D. Sharp, C. W. Yuan, D. O. Yi, C. Y. Liao, A. M. Glaeser, A. M. Minor, J. W. Beeman, M. C. Ridgway, P. Kluth, J. W. Ager, D. C. Chrzan, and E. E. Haller, Phys. Rev. Lett. **97**, 155701 (2006).
[25] E. Bugiel, *Specimen Preparation for Transmission Electron Microscopy of Materials IV*, MRS Symposia Proceedings No. 480, edited by R. M. Anderson and S. D. Walck, (Materials Research Society, Pittsburgh, 1997), p. 89.
[26] W. Ostwald, Z. Elektrochem. Angew. Phys. Chem. **34**, 495 (1900).
[27] C. Spinella, S. Lombardo, and F. Priolo, J. Appl. Phys. **84**, 5383 (1998).
[28] G. V. Williams, A. Bittar, and H. J. Bittar, J. Appl. Phys. **67**, 1874 (1990).
[29] Y. Wakayama, T. Tagami, and S. Tanaka, Thin Solid Films **350**, 300 (1999).
[30] Y. Tu and J. Tersoff, Phys. Rev. Lett. **84**, 4393 (2000).
[31] The exact choice of the parameter S is of minor importance for the NC formation behavior at beginning outgrowth from the initial layer since the decrease in the initial layer thickness d_0 [Eq.(A2)] is very small at this point.
[32] I. D. Sharp, D. O. Yi, Q. Xu, C. Y. Liao, J. W. Beerman, Z. Liliental-Weber, K. M. Yu, D. N. Zakharov, J. W. Ager III, D. C. Chrzan, and E. E. Haller, Appl. Phys. Lett. **86**, 063107 (2005).
[33] AFM measurements as well as cross-section TEM investigations yielded no roughening of the top SiO_2 surface after nanocrystal formation.
[34] N. Kaiser, A. Cröll, F. R. Szofran, S. D. Cobb, and K. W. Benz, J. Cryst. Growth **231**, 448 (2001).
[35] H. Kajiyama, S. I. Muramatsu, T. Shimada, and Y. Nishino, Phys. Rev. B **45**, 14005 (1992).
[36] J. K. Bording and J. Taftoo, Phys. Rev. B **62**, 8098 (2000).
[37] J. B. Johnson and K. G. McKay, Phys. Rev. **93**, 668 (1954).
[38] Y. C. Yong, J. T. L. Thong, and J. C. H. Phang, J. Appl. Phys. **84**, 4543 (1998).
[39] I. M. Lifshitz and V. V. Slyozov, J. Phys. Chem. Solids **19**, 35 (1961); C. Wagner, Z. Elektrochem. **65**, 581 (1961).
[40] D. Riabinina, C. Durand, J. Margot, M. Chaker, G. A. Botton, and F. Rosei, Phys. Rev. B **74**, 075334 (2006).